Constraints on Sterile Neutrino Models from Strong Gravitational Lensing, Milky Way Satellites, and the Lyman-α Forest

Ioana A. Zelko,[1,*] Tommaso Treu,[1] Kevork N. Abazajian,[2] Daniel Gilman,[3] Andrew J. Benson,[4] Simon Birrer,[5,6] Anna M. Nierenberg,[7] and Alexander Kusenko[1,8]

[1]*Department of Physics and Astronomy, University of California, Los Angeles, 475 Portola Plaza, Los Angeles, California 90095, USA*

[2]*Department of Physics and Astronomy, University of California, Irvine, Irvine, California 92697, USA*

[3]*Department of Astronomy and Astrophysics, University of Toronto, 50 St. George Street, Toronto, Ontario, M5S 3H4, Canada*

[4]*Observatories of the Carnegie Institution for Science, 813 Santa Barbara Street, Pasadena, California 91101, USA*

[5]*Kavli Institute for Particle Astrophysics and Cosmology and Department of Physics, Stanford University, Stanford, California 94305, USA*

[6]*SLAC National Accelerator Laboratory, Menlo Park, California 94025, USA*

[7]*University of California Merced, Department of Physics 5200 North Lake Road, Merced, California 95343, USA*

[8]*Kavli IPMU (WPI), UTIAS, The University of Tokyo, Kashiwa, Chiba 277-8583, Japan*

(Received 24 March 2022; revised 3 August 2022; accepted 20 September 2022; published 4 November 2022; corrected 16 December 2022)

The nature of dark matter is one of the most important unsolved questions in science. Some dark matter candidates do not have sufficient nongravitational interactions to be probed in laboratory or accelerator experiments. It is thus important to develop astrophysical probes which can constrain or lead to a discovery of such candidates. We illustrate this using state-of-the-art measurements of strong gravitationally lensed quasars to constrain four of the most popular sterile neutrino models, and also report the constraints for other independent methods that are comparable in procedure. First, we derive effective relations to describe the correspondence between the mass of a thermal relic warm dark matter particle and the mass of sterile neutrinos produced via Higgs decay and grand unified theory (GUT)-scale scenarios, in terms of large-scale structure and galaxy formation astrophysical effects. Second, we show that sterile neutrinos produced through the Higgs decay mechanism are allowed only for mass > 26 keV, and GUT-scale scenario > 5.3 keV. Third, we show that the single sterile neutrino model produced through active neutrino oscillations is allowed for mass > 92 keV, and the three sterile neutrino minimal standard model (νMSM) for mass > 16 keV. These are the most stringent experimental limits on these models.

DOI: 10.1103/PhysRevLett.129.191301

Introduction.—The nature of dark matter (DM) is one of the most important questions in modern physics, with implications spanning from particle physics to astrophysics and cosmology. This unknown particle contributes 25% of the total energy of the universe [1], but is not made of ordinary matter and has no electromagnetic interaction.

Many DM models have been proposed. A number of candidates fall into the class of cold dark matter (CDM) [2], made of collisionless particles considered "cold" due to their small velocity dispersion relative to the speed of light. This model is extremely successful on supergalactic scales but there are open challenges at subgalactic scales [3]. CDM predicts more satellites than are observed around galaxies of Milky Way (MW) mass, "cuspy" dark matter density profiles in contrast to the flatter cores observed in dwarf galaxies and clusters, and predicts that subhalos hosting the largest MW satellites are either underdense or too small. It is still unclear whether these challenges can be solved by a better understanding of baryonic processes, or whether alternative dark matter models are needed (e.g., [4] and references therein).

Plenty of DM models have been proposed to eliminate these small-scale tensions between observations and CDM [5]. DM particles which are generated with higher velocity dispersions erase fluctuations in the matter power spectrum at scales smaller than a characteristic "free-streaming length," suppressing structures below this scale. So-called "hot" dark matter candidates such as standard neutrinos are ruled out by observations [6–9], as the main DM component. However, a broad range of "warm" DM (WDM) with smaller but non-negligible free streaming lengths are viable. One popular class of WDM models are sterile neutrinos (SNs).

Sterile neutrinos [10–14] are particles with right-handed chirality, no charge, and no color charge, and therefore do not interact with standard model particles except via mixing with neutrinos, or via some non-standard-model interactions. They were first introduced for the purpose of explaining the masses of active (left-handed) neutrinos, and can have masses in the range from eV to the Planck scale. In the early universe they can decouple from the plasma before electron-positron annihilation, when they are still relativistic [12,15–18].

The exact production mechanism for a given SN model determines the clustering of dark matter [19–22]. The Dodelson and Widrow [23] (hereafter the DW) model adds a single SN with coupling to active neutrinos. DW SNs are produced in neutrino oscillations at temperatures below a few GeV [24].

Alternatively, there may be multiple SN species produced in neutrino oscillations. In the seesaw theory of neutrino masses, one needs at least two right-handed states [25], but more right-handed states are allowed. In the presence of a sizable lepton asymmetry, the active to SNs conversions select a lower-momentum part of the thermal distribution, leading to somewhat colder dark matter [Shi and Fuller (SF), [26]]. Thus, the popular neutrino minimal standard model [[26,27], hereafter νMSM or SF] postulates three right-handed neutrinos with masses below the electroweak scale.

SNs could also be produced through mechanisms other than active neutrino oscillations, including "freeze-in" production from decays of the inflaton [28] or an $\mathrm{SU}(2) \times \mathrm{U}(1)$ singlet Higgs boson [PK, [19–22]]. Most of the SN production from oscillations (DW or SF) takes place at temperature $\sim$0.1 GeV. In contrast, Higgs boson decays can produce a population of SNs at a temperature $\sim$100 GeV. Subsequent cooling and entropy production dilutes and redshifts this population, making the resulting DM colder than the WDM produced by DW or SF models. This model, which produces particles in the 1–10 keV range, has been shown to produce the correct dark matter abundance, resulting in the so-called "keV miracle model" (hereafter PK).

Another possible production mechanism for SNs is the split seesaw mechanism [[29], hereafter KTY]. The model predicts two large Majorana masses and one small Majorana mass due to a natural separation of scales. The large Majorana masses allow for thermal leptogenesis, while the keV mass produces a DM candidate. The model can be embedded into an SO(10) grand unified theory (GUT), or some other theory containing a gauge $\mathrm{U}(1)_{B-L}$ symmetry. The resulting DM is colder than the models described above, due to dilution and redshifting of SNs as the plasma cools from the GUT-scale production temperature.

The four SN models described above could explain the unidentified 3.5 keV x-ray line found in observations of galaxies and clusters [30,31], even if they do not account for 100% of DM. Furthermore, keV SNs can have a dramatic effect on supernovae, e.g., explaining the pulsar kick velocities in excess of 1000 km/s which so far has evaded other explanations [32,33].

We use state-of-the-art measurements of gravitationally lensed quasars [34,35], as [36–38] MW satellites [39–42], and Lyα [43,44], to constrain the four popular SN models described above. We take their limits in terms of the thermal relic WDM, and compute the equivalent limits for the four SN models described above, from the point of view of cosmological structure formation and the halo mass function. As we will show, our analysis provides the most stringent limits to date on these four SN models.

Thermal relic warm dark matter constraints from strong gravitational lensing.—Strong gravitational lensing depends only upon gravity and is thus sensitive to the abundance of halos irrespective of their ability to emit or absorb light. It can thus determine the halo mass function directly, avoiding uncertainties related to the physics of star formation in low mass galaxies that affect traditional methods.

Reference [35] used eight quadruply imaged quasar systems to constrain the amplitude of the halo mass function and the free-streaming length of dark matter. For each system, many realizations of dark matter structure are drawn from analytic dark matter halo mass functions flexible enough to describe mass functions produced by a broad range of thermal relic dark matter masses.

The predicted flux ratios for each realization are compared with the observed flux ratios to estimate the likelihood using approximate Bayesian computing. The likelihoods from each system are multiplied together to infer the parameters common to all systems. A key parameter is the "half-model mass" m_{HM} which is the mass at which there are half as many halos as there would have been in the case of CDM.

We marginalize over all the other parameters to obtain the posterior distribution for m_{HM}. As always in Bayesian statistics, the posterior depends on the choice of priors. Since we do not know the order of magnitude of the SN mass we adopt a uniform prior in $\log 10(m_{\mathrm{HM}})$, within the range $10^{4.8} - 10^{10}\ M_{\odot}$ (reported in units of Sun mass following existing literature on the halo mass function).

The constraints on m_{HM} can be tied into constraints on the mass of the DM particle, given a model. A traditional reference model is the thermal relic WDM. It does not refer to a physical particle in particular, but serves as a standard tie-in model for the properties of WDM models with thermal relics. References [45] and [46] derived a one-to-one mapping between the half-mode mass and the mass of the thermal relic WDM. The general form of the conversion is

$$m_{\mathrm{thWDM}} = 3.3 \left[\left(\frac{m_{\mathrm{HM}}[M_{\odot}]}{A} \right)^{-1/3.33} \right] \mathrm{keV}, \qquad (1)$$

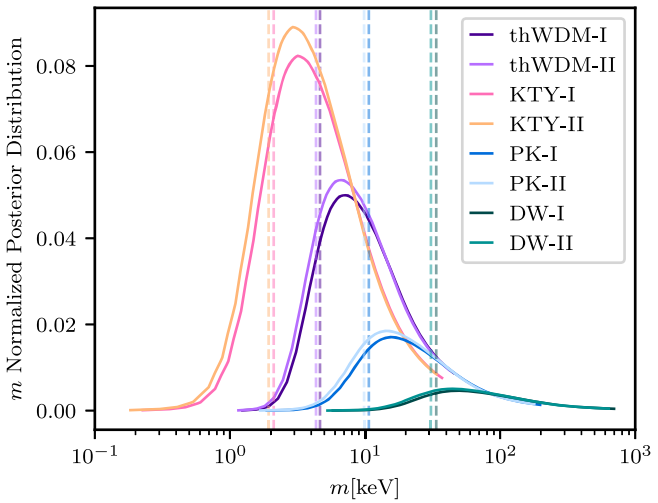

FIG. 1. Posterior probability distribution function $p(m)$ of the mass of thermal relic WDM and the various kinds of SN: the GUT-scale scenario (KTY), the "keV miracle model" Higgs production mechanism (PK), and single particle neutrino oscillation production mechanism (DW). The posteriors do not go to 0 on the right limit, so we cannot impose upper constraints on the particle masses; however, since they do go to 0 on the small limit, we can derive a lower limit. The vertical dashed line marks the 95% lower boundary interval, corresponding to 4.6, 2.1, 11, 34 keV for thWDM, KTY, PK, DW. The limits for the νMSM model depend on lepton asymmetry, and are discussed in the text. The case where the assumption for the average background density of the universe includes [case (i)], or does not include [case (ii)], baryonic matter in addition to dark matter (see Appendix in the Supplemental Material [47]) is shown.

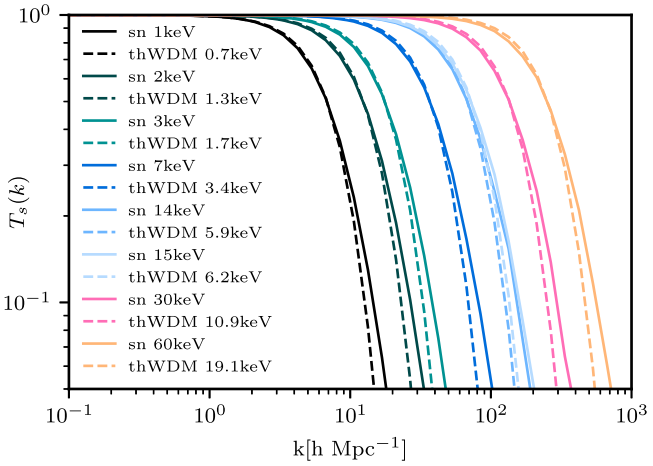

FIG. 2. SN transfer functions belonging to the Higgs decay (PK) model proposed by [20], shown by the continuous lines. The dashed lines show the corresponding thermal relic WDM transfer functions. As shown in [22], the two sets of functions are very similar to each other, thus allowing the possibility to create a mapping between the masses of thermal relic WDM particles and those of SNs.

where A has two possible values [case (i) and case (ii)], depending on assumptions about the background density of the universe, as detailed in the Appendix in the Supplemental Material. Using Eq. (1), we obtain the posterior shown in Fig. 1.

Relation between thermal relic WDM and sterile neutrino transfer functions.—Our goal is to use the constraints discussed as an illustration in the section "Thermal relic warm dark matter constraints from strong gravitational lensing," and those obtained by [42] and [43,44] to derive constraints on the four SN dark matter candidates discussed in the Introduction: the GUT-scale scenario (KTY), the "keV miracle model" Higgs production mechanism (PK), the single particle neutrino oscillation production mechanism (DW), and the Shi-Fuller mechanism within the neutrino minimal standard model (νMSM).

The key quantity is the transfer function, T, which describes the effect of free-streaming on matter distribution. Given the power spectrum of initial density fluctuations P_i, T describes its evolution as a function of scale k and cosmic time, with respect to a standard CDM model: $T_s(k) \equiv \sqrt{[P_{\text{sterile},i}(k)/P_{\text{CDM},i}(k)]}$.

Transfer functions for SNs (Fig. 2) for the Higgs production mechanism and the GUT-scale scenarios have been previously obtained by [22]. We calculate the transfer functions of several models by using the momentum-space distribution functions as tables that are provided to CLASS. Including these with the proper effective temperature of the dark matter models allows for accurate calculation of the transfer functions relative to CDM. The ones given here supersede the published ones by adopting more up to date cosmological parameters. We also corrected a mismatch between expected and provided dilution factors, using the non-CDM features of CLASS [50]. For the initial conditions, we fix the cosmology to the mean results from [1] and the cosmic microwave background temperature from [51].

The thermal relic WDM transfer functions for a given m_{thWDM} can be obtained from the analytical form presented in equation A9 of [45] (with more recent numbers from [48]), and it is given by

$$T_{\text{thWDM}}(k) = [1 + (\alpha k)^{2\mu}]^{-5/\mu} \tag{2}$$

with α, μ given in the Appendix in the Supplemental Material.

We tested two methods to find the relation between SN and thermal relic WDM transfer functions: first, we fit the SN transfer functions using the mass of the thermal relic WDM as a free parameter [Eq. (2)]; second, we match the "half-mode" wave number where the transfer functions decrease to 0.5. The half-mode k_{HM} and the mass of the particle m_{thWDM} can be related analytically from Eq. (2), to obtain

$$m_{\text{thWDM}} = k_{\text{HM}}^{\frac{1}{1.11}} \left[0.049 (2^{\frac{\mu}{5}} - 1)^{-\frac{1}{2\mu}} \times \left(\frac{\Omega_X}{0.25} \right)^{0.11} \left(\frac{h}{0.7} \right)^{1.22} \right]^{\frac{1}{1.11}}. \tag{3}$$

TABLE I. Coefficients for the fits for the relation between the $m_{\rm SN}$ and $m_{\rm thWDM}$, for the cases of the Higgs production mechanism (PK) and GUT scale (KTY). The power law fit, as well as the first two degree polynomials are shown.

	deg	a_0	a_1	a_2
PK	First	$-3.26e+00$	$3.21e+00$	
	Second	$-1.06e+00$	$2.31e+00$	$4.66e-02$
KTY	First	$-1.10e+00$	$6.87e-01$	
	Second	$-4.17e-01$	$5.11e-01$	$7.15e-03$
Power law		a	b	
PK		$1.56e+00$	$1.24e+00$	
KTY		$3.14e-01$	$1.24e+00$	

In the first method, the fits might depend too much on how the numerical $T(k)$ for the SNs was sampled, and the errors that arise at high k. The 1/2 mode matching gets rid of those issues, so we use this one for the rest of the Letter. The difference in the end results of the two methods is of order 1%. We obtain the fits shown in Fig. 2. For root-mean-square goodness of fit estimator, the PK model KTY model were comparable.

The relation between the mass of the SN which generates an equivalent transfer function to a thermal relic particle with a given mass can be approximated by a polynomial of degree deg, $m_{\rm SN} = f(m_{\rm thWDM}) = \sum_0^{\rm deg} a_i \cdot m_{\rm thWDM}^i$, or by a power law $m_{\rm SN} = a \cdot m_{\rm thWDM}^b$.

Results of the polynomial fits of orders 1, 2 (higher orders resulted in over fitting), as well as the power law, can be seen in Table I. Using these coefficients, a relation can also be derived between $m_{\rm SN}$ and $m_{\rm HM}$, seen below in the case of the power law fit:

$$m_{\rm SN} = a \cdot 3.3^b \left(\frac{m_{\rm HM}}{A}\right)^{-b/3.33} \tag{4}$$

where A takes the values described in the Appendix in the Supplemental Material. These relations are calibrated on the $m_{\rm thWDM}$ mass interval of (0.75, 22) keV, and then extended to 60 keV when applied to data. Figure 3 shows the results of these fits. We use the results of the second order polynomial but we note that using a linear approximation would change the inferred bounds on the SN mass by only 11%.

This mapping allows one to convert any results obtained for thermal relic WDM to SN in postprocessing, without redoing the experiment or the analysis.

For SNs produced through the oscillation mechanism for the Dodelson-Widrow model, the relation between $m_{\rm SN}$ and $m_{\rm thWDM}$ is taken from [48].

For the νMSM model, [52] derives the model connections to the half-mode mass $m_{\rm HM}$, and we use the $m_{\rm HM}$ posterior to constrain them.

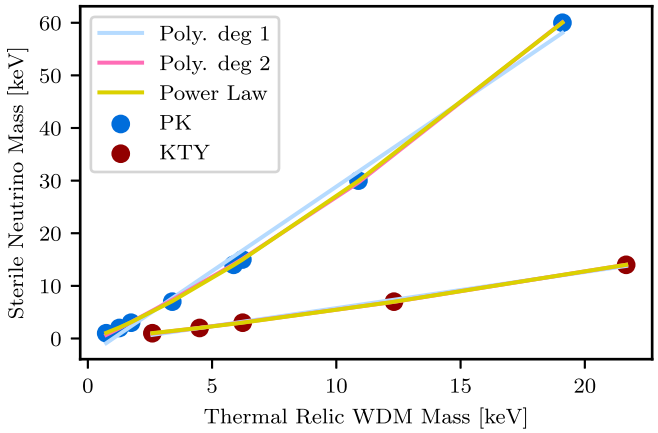

FIG. 3. The masses of the thermal relic WDM particles and SN particles corresponding to the PK transfer functions shown in Fig. 2, as well as those for the KTY model, are shown as scattered points. Polynomial and power-law fits are shown as solid lines. These relations allow us to map constraints on the mass of thermal relic WDM to the corresponding mass of a SN, for the Higgs production mechanism (PK), and the GUT-scale scenario (KTY).

Mapping thermal relic warm dark matter constraints onto sterile neutrinos.—We obtain the most stringent experimental limits on four SN models: PK, KTY, νMSM, and DW.

To recap, our starting points are the following 95% confidence limits on thermal relic WDM. The lensing-only analysis described in section "Thermal relic warm dark matter constraints from strong gravitational lensing" gives $m_{\rm thWDM} > 4.6$ keV [35]. Combination with satellite counts extends it to $m_{\rm thWDM} > 9.7$ keV [42]. Independent work on the Lyman-α forest yields 3.3 keV [43] and 5.3 keV [44], the latter using additional assumptions for the relevant thermodynamics.

For the PK and KTY models, the relations derived in section "Relation between thermal relic WDM and sterile neutrino transfer functions" can now be used together with the ones for νMSM and DW to translate limits from thermal relic WDM into limits for the SNs masses (Fig. 1). The 95% limits for the four models are given in Table II.

We note that the posterior shown in Fig. 1 vanishes at the lower bound but not on the upper bound, as expected because the warmest models are ruled out by a number of observations [8,9,42]. This puts a lot of weight on the choice of priors, which can influence the limits reported. We thus convert the posteriors to lower limits, although of course the full posterior is more informative. Likelihood ratios can be obtained from Fig. 1.

For the νMSM model, we use the posterior on $m_{\rm HM}$ to eliminate the model space as shown in Fig. 2 of [52], which presents the expected half-mode mass as a function of lepton asymmetry (L6) for different neutrino masses. Our upper limit on $\log_{10}(m_{\rm HM}[M_\odot])$ from strong lensing

TABLE II. 95% lower limits for four sterile neutrino models: Higgs production mechanism (PK), GUT scale scenario (KTY), three sterile neutrino minimal standard model (νMSM), single model sterile neutrino produced through active neutrino oscillations (DW). The limits are derived from four datasets: gravitational strong lensing [35], strong lensing combined with Milky Way galaxy counts [42], Lyman-α forest [43], and Lyman-α forest combined with thermodynamic assumptions [44]. The case (i) and case (ii) labels correspond to different assumption cases about the average background density of the universe, as described in the Appendix. In the last two rows of the table, we also present the limits in terms of the half-mode mass, and the thermal relic WDM mass.

	Strong lensing	Strong lensing and galaxy counts	Lyman-α	Lyman-α and Thermo.
PK (keV)	I: 11, II: 9.8	I: 26, II: 24	7.1	12
KTY (keV)	I: 2.1, II: 1.9	I: 5.3, II: 4.9	1.3	2.5
νMSM (keV)	7.0	16	I: 5.0, II: 5.0	I: 9.0, II: 10
DW (keV)	I: 34, II: 31	I: 92, II: 84	21	40
$\log_{10}(\mathrm{HM}[M_\odot])$	8.1	7.0	I: 8.6, II: 8.5	I: 7.9, II: 7.8
thWDM (keV)	I: 4.6, II: 4.3	I: 9.8, II: 9.2	3.3	5.3

alone is 8.1. This rules out masses under 7.0 keV for all lepton asymmetries. For higher masses, only limited ranges of lepton asymmetries are allowed: 7 keV: $\mathrm{L6} \in (6.8, 7.6)$, 9 keV: $\mathrm{L6} \in (5.2, 7.8)$, 11 keV: $\mathrm{L6} \in (4.3, 7.6)$, 14 keV: $\mathrm{L6} \in (1.7, 7.9)$, 16 keV: $\mathrm{L6} \in (1.6, 11.5)$. After incorporating the MW satellite count constraints, $\log_{10}(m_{\mathrm{HM}}[M_\odot]) > 7.0$, which corresponds to $m_{\nu\mathrm{MSM}} > 16$ keV. These limits are improved compared to existing work ([53]). These results are contingent on the assumption that DM is made from a single component, the SN model of choice. However, DM could be a mixture of different components, such as the "mixed cold + warm DM model" [54,55]. Adding a parameter to control the abundance ratio could make the constraints weaker.

Future work would aim to combine the limits from strong lensing, galaxy counts, and the Lyman-α forest in a joint analysis. Work has already been done in this direction ([56]), however their dataset obtained less stringent limits than the strong lensing combined with galaxy counts obtained by [42]. Future analysis combining the datasets used in Table II will be useful. In addition, work exploring analytical connections in the nonlinear regime (as was done at the level of the transfer function by [57]) at the subhalo level would be useful.

Conclusion.—We used flux ratios of strong gravitationally lensed quasars, MW satellites, and the Lyman-α forest to constrain four of the most popular SN models.

First, we derive effective relations to describe the correspondence between the mass of a thermal relic WDM particle and the mass of SNs produced via Higgs decay and GUT-scale scenarios, in terms of astrophysical effects. We take advantage of the similarity between the transfer functions of the SNs mechanism presented by [22], to that of thermal relic WDM.

We note that our derived equivalence relations are of general importance, and can be used to put limits on SN models for any thermal relic WDM measurement, not just the ones we present here.

The limits on the PK, KTY, νMSM, and DW models summarized in Table II are the most stringent experimental limits on these four models. We note that the limits from lensing and MW satellites are independent of and agree with those from the Lyα forest. We have effectively ruled out part of the parameter space for SNs generated through these four models.

The code and data for this project can be found at [58].

We are grateful to the three anonymous referees for their very useful suggestions that lead to the improvement of the manuscript. We acknowledge helpful conversations with Graciela Gelmini, Jiamin Hou, Doug Finkbeiner, Ethan Nadler, Joshua Speagle, and Xiaolong Du. We are also grateful to the three anonymous referees for their useful suggestions that improved the manuscript. I. Z. and T. T. acknowledge support by the National Science Foundation Grant No. NSF-1836016, by the Gordon and Betty Moore Foundation Grant 8548 and by NASA Grant No. HST-GO-15177. Part of the data used in this Letter were obtained as part of HST-GO-15177. S. B. is supported by the National Science Foundation through NSF AST-1716527. K. N. A. is supported in part by NSF Theoretical Physics Grant PHY-1915005. A. K. was supported by the U.S. Department of Energy (DOE) Grant No. DE-SC0009937 and by Japan Society for the Promotion of Science (JSPS) KAKENHI grant No. JP20H05853, as well as by World Premier International Research Center Initiative (WPI), MEXT, Japan. This work was supported in part by the UC Southern California Hub, with funding from the UC National Laboratories division of the University of California Office of the President. This research made use of the NASA Astrophysics Data System's Bibliographic Services (ADS), the color blindness palette by Martin Krzywinski and Jonathan Corum [59], the Color Vision Deficiency PDF Viewer by Marie Chatfield [60], and the following software: CLASS [61], JUPYTER NOTEBOOK [62], MATHEMATICA [63], MATPLOTLIB [64], NumPy [65], PYTHON [66,67], SCIKIT- LEARN [68].

*Corresponding author.
ioana.zelko@gmail.com

[1] Planck Collaboration, Planck 2018 results. VI. Cosmological parameters, Astron. Astrophys. **641**, A6 (2020).
[2] G. R. Blumenthal, S. M. Faber, J. R. Primack, and M. J. Rees, Formation of galaxies and large-scale structure with cold dark matter, Nature (London) **311**, 517 (1984).
[3] J. S. Bullock and M. Boylan-Kolchin, Small-scale challenges to the ΛCDM paradigm, Annu. Rev. Astron. Astrophys. **55**, 343 (2017).
[4] D. H. Weinberg, J. S. Bullock, F. Governato, R. Kuzio de Naray, and A. H. G. Peter, Cold dark matter: Controversies on small scales, Proc. Natl. Acad. Sci. U.S.A. **112**, 12249 (2015).
[5] M. S. Seigar, *Dark Matter in the Universe* (Morgan & Claypool Publishers, 2015).
[6] O. E. Gerhard and D. N. Spergel, Dwarf spheroidal galaxies and the mass of the neutrino, Astrophys. J. **389**, L9 (1992).
[7] J. R. Primack, J. Holtzman, A. Klypin, and D. O. Caldwell, Cold + Hot Dark Matter Cosmology with m(νμ)≈m(ντ)≈2.4ev, Phys. Rev. Lett. **74**, 2160 (1995).
[8] N. Menci, A. Merle, M. Totzauer, A. Schneider, A. Grazian, M. Castellano, and N. G. Sanchez, Fundamental physics with the Hubble frontier fields: Constraining dark matter models with the abundance of extremely faint and distant galaxies, Astrophys. J. **836**, 61 (2017).
[9] J. W. Hsueh, W. Enzi, S. Vegetti, M. W. Auger, C. D. Fassnacht, G. Despali, L. V. E. Koopmans, and J. P. McKean, SHARP—VII. New constraints on the dark matter free-streaming properties and substructure abundance from gravitationally lensed quasars, Mon. Not. R. Astron. Soc. **492**, 3047 (2020).
[10] A. Kusenko, Sterile neutrinos: The dark side of the light fermions, Phys. Rep. **481**, 1 (2009).
[11] K. N. Abazajian *et al.*, Light Sterile Neutrinos: A White Paper (2012).
[12] K. N. Abazajian, Sterile neutrinos in cosmology, Phys. Rep. **711**, 1 (2017).
[13] R. Adhikari *et al.*, A white paper on keV sterile neutrino dark matter, J. Cosmol. Astropart. Phys. 01 (2017) 025.
[14] A. Boyarsky, M. Drewes, T. Lasserre, S. Mertens, and O. Ruchayskiy, Sterile neutrino dark matter, Prog. Part. Nucl. Phys. **104**, 1 (2019).
[15] R. A. Malaney and G. M. Fuller, Sterile neutrinos in the early universe, in *Primordial Nucleosynthesis and Evolution of Early Universe* (AA[Lawrence Livermore National Laboratory, California], AB[University of California, San Diego], 1991), Vol. 169, p. 91.
[16] S. Hannestad, I. Tamborra, and T. Tram, Thermalisation of light sterile neutrinos in the early universe, J. Cosmol. Astropart. Phys. 07 (2012) 025.
[17] S. Gariazzo, P. F. de Salas, and S. Pastor, Thermalisation of sterile neutrinos in the early universe in the 3 + 1 scheme with full mixing matrix, J. Cosmol. Astropart. Phys. 07 (2019) 014.
[18] G. Alonso-Álvarez and J. M. Cline, Sterile neutrino production at small mixing in the early universe, Phys. Lett. B **833**, 137278 (2022).
[19] A. Kusenko, Sterile Neutrinos, Dark Matter, and Pulsar Velocities in Models with a Higgs Singlet, Phys. Rev. Lett. **97**, 241301 (2006).
[20] K. Petraki and A. Kusenko, Dark-matter sterile neutrinos in models with a gauge singlet in the Higgs sector, Phys. Rev. D **77**, 065014 (2008).
[21] K. Petraki, Small-scale structure formation properties of chilled sterile neutrinos as dark matter, Phys. Rev. D **77**, 105004 (2008).
[22] K. N. Abazajian and A. Kusenko, Hidden treasures: Sterile neutrinos as dark matter with miraculous abundance, structure formation for different production mechanisms, and a solution to the σ_8 problem, Phys. Rev. D **100**, 103513 (2019).
[23] S. Dodelson and L. M. Widrow, Sterile Neutrinos as Dark Matter, Phys. Rev. Lett. **72**, 17 (1994).
[24] K. Abazajian, Linear cosmological structure limits on warm dark matter, Phys. Rev. D **73**, 063513 (2006).
[25] P. H. Frampton, S. L. Glashow, and T. Yanagida, Cosmological sign of neutrino *CP* violation, Phys. Lett. B **548**, 119 (2002).
[26] X. Shi and G. M. Fuller, New Dark Matter Candidate: Nonthermal Sterile Neutrinos, Phys. Rev. Lett. **82**, 2832 (1999).
[27] T. Asaka and M. Shaposhnikov, The @nMSM, dark matter and baryon asymmetry of the universe [rapid communication], Phys. Lett. B **620**, 17 (2005).
[28] M. Shaposhnikov and I. Tkachev, The nuMSM, inflation, and dark matter, Phys. Lett. B **639**, 414 (2006).
[29] A. Kusenko, F. Takahashi, and T. T. Yanagida, Dark matter from split seesaw, Phys. Lett. B **693**, 144 (2010).
[30] E. Bulbul, M. Markevitch, A. Foster, R. K. Smith, M. Loewenstein, and S. W. Randall, Detection of an unidentified emission line in the stacked x-ray spectrum of galaxy clusters, Astrophys. J. **789**, 13 (2014).
[31] A. Boyarsky, O. Ruchayskiy, D. Iakubovskyi, and J. Franse, Unidentified Line in X-Ray Spectra of the Andromeda Galaxy and Perseus Galaxy Cluster, Phys. Rev. Lett. **113**, 251301 (2014).
[32] A. Kusenko and G. Segre, Neutral current induced neutrino oscillations in a supernova, Phys. Lett. B **396**, 197 (1997).
[33] G. M. Fuller, A. Kusenko, I. Mocioiu, and S. Pascoli, Pulsar kicks from a dark-matter sterile neutrino, Phys. Rev. D **68**, 103002 (2003).
[34] T. Treu, Strong lensing by galaxies, Annu. Rev. Astron. Astrophys. **48**, 87 (2010).
[35] D. Gilman, S. Birrer, A. Nierenberg, T. Treu, X. Du, and A. Benson, Warm dark matter chills out: Constraints on the halo mass function and the free-streaming length of dark matter with eight quadruple-image strong gravitational lenses, Mon. Not. R. Astron. Soc. **491**, 6077 (2020).
[36] A. M. Nierenberg, D. Gilman, T. Treu, G. Brammer, S. Birrer, L. Moustakas, A. Agnello, T. Anguita, C. D. Fassnacht, V. Motta, A. H. G. Peter, and D. Sluse, Double dark matter vision: Twice the number of compact-source lenses with narrow-line lensing and the WFC3 grism, Mon. Not. R. Astron. Soc. **492**, 5314 (2020).
[37] A. M. Nierenberg, T. Treu, G. Brammer, A. H. G. Peter, C. D. Fassnacht, C. R. Keeton, C. S. Kochanek, K. B. Schmidt, D. Sluse, and S. A. Wright, Probing dark matter

substructure in the gravitational lens HE 0435-1223 with the WFC3 grism, Mon. Not. R. Astron. Soc. **471**, 2224 (2017).
[38] A. M. Nierenberg, T. Treu, S. A. Wright, C. D. Fassnacht, and M. W. Auger, Detection of substructure with adaptive optics integral field spectroscopy of the gravitational lens B1422 + 231, Mon. Not. R. Astron. Soc. **442**, 2434 (2014).
[39] A. Schneider, Astrophysical constraints on resonantly produced sterile neutrino dark matter, J. Cosmol. Astropart. Phys. 04 (2016) 059.
[40] J. F. Cherry and S. Horiuchi, Closing in on resonantly produced sterile neutrino dark matter, Phys. Rev. D **95**, 083015 (2017).
[41] E. O. Nadler *et al.* (DES Collaboration), Constraints on Dark Matter Properties from Observations of Milky Way Satellite Galaxies, Phys. Rev. Lett. **126**, 091101 (2021).
[42] E. O. Nadler, S. Birrer, D. Gilman, R. H. Wechsler, X. Du, A. Benson, A. M. Nierenberg, and T. Treu, Dark matter constraints from a unified analysis of strong gravitational lenses and milky way satellite galaxies, Astrophys. J. **917**, 7 (2021).
[43] M. Viel, G. D. Becker, J. S. Bolton, and M. G. Haehnelt, Warm dark matter as a solution to the small scale crisis: New constraints from high redshift Lyman-α forest data, Phys. Rev. D **88**, 043502 (2013).
[44] V. Iršič, M. Viel, M. G. Haehnelt, J. S. Bolton, S. Cristiani, G. D. Becker, V. D'Odorico, G. Cupani, T.-S. Kim, T. A. M. Berg, S. López, S. Ellison, L. Christensen, K. D. Denney, and G. Worseck, New constraints on the free-streaming of warm dark matter from intermediate and small scale Lyman-α forest data, Phys. Rev. D **96**, 023522 (2017).
[45] P. Bode, J. P. Ostriker, and N. Turok, Halo formation in warm dark matter models, Astrophys. J. **556**, 93 (2001).
[46] A. Schneider, R. E. Smith, A. V. Macciò, and B. Moore, Non-linear evolution of cosmological structures in warm dark matter models, Mon. Not. R. Astron. Soc. **424**, 684 (2012).
[47] See the Supplemental Material at http://link.aps.org/supplemental/10.1103/PhysRevLett.129.191301 for the Appendix describing the relation between the half-mode mass m_{HM} and the thermal relic WDM mass m_{thWDM}, which includes Refs. [35,39,42,43,45,46].
[48] M. Viel, J. Lesgourgues, M. G. Haehnelt, S. Matarrese, and A. Riotto, Constraining warm dark matter candidates including sterile neutrinos and light gravitinos with WMAP and the Lyman-α forest, Phys. Rev. D **71**, 063534 (2005).
[49] M. Viel, K. Markovič, M. Baldi, and J. Weller, The non-linear matter power spectrum in warm dark matter cosmologies, Mon. Not. R. Astron. Soc. **421**, 50 (2012).
[50] D. Blas, J. Lesgourgues, and T. Tram, The cosmic linear anisotropy solving system (CLASS). Part II: Approximation schemes, J. Cosmol. Astropart. Phys. 07 (2011) 034.
[51] D. J. Fixsen, The temperature of the cosmic microwave background, Astrophys. J. **707**, 916 (2009).
[52] S. Vegetti, G. Despali, M. R. Lovell, and W. Enzi, Constraining sterile neutrino cosmologies with strong gravitational lensing observations at redshift $z = 0.2$, Mon. Not. R. Astron. Soc. **481**, 3661 (2018).
[53] A. Dekker, S. Ando, C. A. Correa, and K. C. Y. Ng, Warm Dark Matter Constraints Using Milky-Way Satellite Observations and Subhalo Evolution Modeling (2021).
[54] A. Boyarsky, J. Lesgourgues, O. Ruchayskiy, and M. Viel, Lyman-α constraints on warm and on warm-plus-cold dark matter models, J. Cosmol. Astropart. Phys. (2009) 012.
[55] J. Baur, N. Palanque-Delabrouille, C. Yèche, A. Boyarsky, O. Ruchayskiy, É. Armengaud, and J. Lesgourgues, Constraints from Ly-α forests on non-thermal dark matter including resonantly-produced sterile neutrinos, J. Cosmol. Astropart. Phys. 12 (2017) 013.
[56] W. Enzi, R. Murgia, O. Newton, S. Vegetti, C. Frenk, M. Viel, M. Cautun, C. D. Fassnacht, M. Auger, G. Despali, J. McKean, L. V. E. Koopmans, and M. Lovell, Joint constraints on thermal relic dark matter from strong gravitational lensing, the Ly α forest, and Milky Way satellites, Mon. Not. R. Astron. Soc. **506**, 5848 (2021).
[57] R. Murgia, A. Merle, M. Viel, M. Totzauer, and A. Schneider, "Non-cold" dark matter at small scales: A general approach, J. Cosmol. Astropart. Phys. 11 (2017) 046.
[58] https://github.com/ioanazelko/sterile-neutrinos-constraints.git.
[59] http://mkweb.bcgsc.ca/biovis2012/color-blindness-palette.png.
[60] https://mariechatfield.com/simple-pdf-viewer/.
[61] J. Lesgourgues, The Cosmic Linear Anisotropy Solving System (CLASS) I: Overview (2011).
[62] T. Kluyver, B. Ragan-Kelley, F. Pérez, B. Granger, M. Bussonnier, J. Frederic, K. Kelley, J. Hamrick, J. Grout, S. Corlay, P. Ivanov, D. Avila, S. Abdalla, and C. Willing, Jupyter Notebooks—a publishing format for reproducible computational workflows, in *Positioning and Power in Academic Publishing: Players, Agents and Agendas*, edited by F. Loizides and B. Schmidt (IOS Press, Austin, 2016), pp. 87–90.
[63] Wolfram Research Inc, Mathematica, {V}ersion 13.0.0 (2021).
[64] J. D. Hunter, Matplotlib: A 2D graphics environment, Comput. Sci. Eng. **9**, 90 (2007).
[65] S. van der Walt, S. C. Colbert, and G. Varoquaux, The NumPy array: A structure for efficient numerical computation, Comput. Sci. Eng. **13**, 22 (2011).
[66] K. J. Millman and M. Aivazis, Python for scientists and engineers, Comput. Sci. Eng. **13**, 9 (2011).
[67] T. E. Oliphant, Python for scientific computing, Comput. Sci. Eng. **9**, 10 (2007).
[68] F. Pedregosa, G. Varoquaux, A. Gramfort, V. Michel, B. Thirion, O. Grisel, M. Blondel, A. Müller, J. Nothman, G. Louppe, P. Prettenhofer, R. Weiss, V. Dubourg, J. Vanderplas, A. Passos, D. Cournapeau, M. Brucher, M. Perrot, and É. Duchesnay, Scikit-learn: Machine Learning in Python (2012).

Correction: A typographical error in the second sentence of the abstract was introduced during the proof production process and has been fixed.